Robust and Adaptive Teleoperation for Compliant Motion Tasks

Jaeheung Park,* Rui Cortesão,** and Oussama Khatib*

**Stanford University, Robotics Group, 94305-9010 CA, USA, E-mails: {park73, ok}@robotics.stanford.edu.*

***University of Coimbra, Electrical and Computer Engineering Department, Institute of Systems and Robotics (ISR), 3030 Coimbra, Portugal, E-mail: cortesao@isr.uc.pt.*

Abstract

This paper presents a novel teleoperation scheme to control a PUMA robotic manipulator with a Phantom haptic device. Using local force control at the slave robot, contact with soft and hard surfaces is attained with high performance. The control design inserts a virtual spring between the master and slave control systems to generate the desired forces. The closed loop performance is increased by using an active observer and on-line stiffness adaptation to the slave contact environment in its forcefeedback controller.

1 Introduction

Teleoperation is an important capability for a wide range of tasks including telemedicine, telesurgery, space operations, remote manipulation of dangerous objects, and distant work in hostile environments. In contact tasks, reflecting contact forces to the user is vital for effective quality teleoperation and for achieving telepresence.

The literature on teleoperation is very extensive. Simple architectures such as position-force[1] and position-position[2] have limited performance [8],[4]. Various implementations have used addditional information (such as forces and accelerations) to achieve better telepresence [8], [10], [9].

Kim at al. [7] suggested local force feedback (shared compliant control) to provide a compliant slave robot for stiff contact. Zhu and Salcudean([5]) shows that perfect telepresence can be obtained using local force feedback with a 3-channel architecture. However, these local force feedback schemes compensate the contact force without explicit knowledge of the environment.

This paper presents a teleoperation scheme that keeps a position-position structure but improves telepresence using force control on the slave side. The position errors are converted into force commands through a virtual stiffness. This scheme uses a decoupled force controller with active observers, in which the dynamics of the slave robot model mismatches, couplings, noise, and external forces are appropriately handled.

The information of environment stiffness is critical to the force control design. However in teleoperation tasks, the contact states may change abruptly between free space and contact with soft or stiff objects. This scheme uses on-line adaptation of the environment stiffness for fast and smooth transitions between the contact states.

The paper is organized as follows: Section 2 describes the system setup and hardware specifications. Section 3 analyzes the teleoperation scheme, focusing on telepresence and stability issues. The force controller is discussed in Section 4. Manipulator dynamics, decoupled force control and the AOB design are introduced. Section 5 addresses on-line stiffness adaptation, based on force data. Section 6 presents experimental results for three surfaces: a sponge, a book and a desk. Section 7 contains the conclusions of this work.

2 System Setup

Figure 1 contains the photographs of the master and slave devices. The master device is a Phantom 1.0A which has 6 DOF and 3 motors for the first three joints. The haptic device is controlled by a quadric-processor Pentium Pro 200 MHz. The slave robot is a PUMA 560, which has a stiff JR3 force sensor on the end-effector. The PUMA has 6 motors and 6 DOF and is connected to a computer (Pentium II 333 MHz, QNX realtime OS) through a TRC205 controller and a ServoToGo board. The control of the orientation is not considered in this setup. The PUMA robot is controlled so that it has the same orientation in a global frame. Time delay is assumed to be negligible because a local area network is used.

[1] Position commands on the master side and force commands on the slave side.

[2] Only position commands.

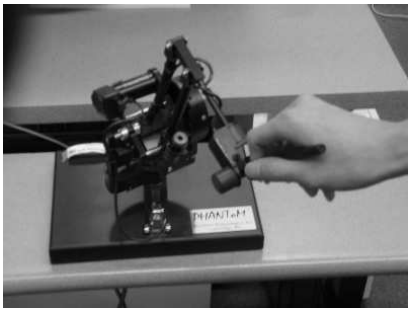

(a)

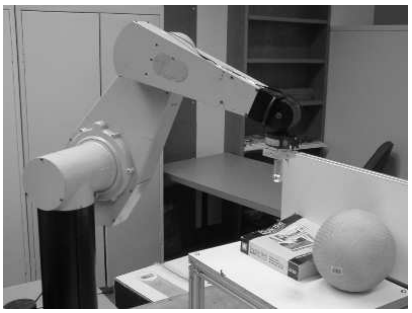

(b)

Figure 1: *System Setup. (a) Phantom™ device controlled by a human. (b) PUMA robot. Soft and stiff objects belong to the PUMA workspace.*

3 Teleoperation Scheme

The PUMA robot is controlled by a decoupled force control method, which will be presented in details at the next section. Therefore, each direction in operational space can be treated independently.

Figure 2 illustrates the teleoperation scheme for each direction in operational space. x_m, x_s, s_p and s_f are the master position, slave position, position scaling and force scaling, respectively. $G_{se}(s)$ represents the slave side, including the robotic manipulator, the force controller and the environment. This scheme is similar to a position-position architecture, where the master and slave exchange their positions as desired positions. However, this scheme has two different aspects. First, the input to the master and slave is the desired force F_d. The force controller commands the slave device to track F_d with a desired dynamics. There is no force feedback controller at the master side. The master haptic device is simply controlled by applying F_d, which is generated by the position error and a virtual spring K_{vir}.

Telepresence is implicitly achieved by the force control. If the end-effector force follows F_d well, the human operator has a very accurate feeling of the real task. Reflecting the desired force has an advantage in the aspect of stability. If the measured environment forces were directly transfered to a master device, they would cause a delay in the loop, and the mass ratio of two systems would significantly limit the stability [4]. However, by feeding back F_d, the master device produces "anticipated" environment forces. Thus, the limitations of position-force scheme are alleviated.

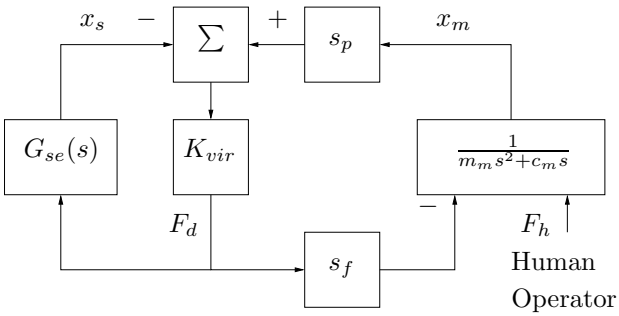

Figure 2: *Teleoperation Scheme.*

Telepresence. Telepresence is analyzed by investigating the transfer function[3] from the human force to the master position [8]

$$\frac{X_m(s)}{F_h(s)}. \tag{1}$$

This transfer function represents the compliance that a human operator feels during teleoperation. When $X_m(s)/F_h(s)$ closely matches the system compliance of the slave robot, telepresence will be provided to the human operator.

From Figure 2,

$$(m_m s^2 + c_m s)X_m = F_h - s_f K_{vir}(s_p X_m - X_s) \tag{2}$$

and

$$G_{se}K_{vir}(s_p X_m - X_s) = X_s, \tag{3}$$

where m_m and c_m are respectively the mass and damping of the master device. For the slave robot, assuming

$$F_c = K_s X_s, \tag{4}$$

where K_s denotes the system stiffness[4] and F_c is the Laplace Transform of contact force,

$$G_{se} = X_s/F_d = \frac{1}{K_s}\frac{F_c}{F_d}. \tag{5}$$

[3]The Laplace transforms of x_m and f_h are $X_m(s)$ and $F_h(s)$, respectively.

[4]If the slave device has very low compliance, K_s is very close to the environment stiffness.

$\frac{F_c}{F_d}$ is the closed loop transfer function of the force control. Therefore, if the force controller has zero steady state errors,

$$G_{se}(s)|_{s=0} = \frac{1}{K_s}. \tag{6}$$

From (2) and (3), (1) is given by

$$\frac{X_m}{F_h} = \frac{K_{vir}+\frac{1}{G_{se}}}{(m_m s^2+c_m s+K_{vir}s_p s_f)(K_{vir}+\frac{1}{G_{se}})-K_{vir}^2 s_p s_f} \quad . \tag{7}$$

Equation (7) can be approximated in two frequency regions:

1. If $|m_m s^2 + c_m s| \ll K_{vir} s_p s_f$ (low frequencies),

$$\frac{X_m}{F_h} \approx \frac{K_{vir}+\frac{1}{G_{se}}}{K_{vir}s_p s_f \frac{1}{G_{se}}} \quad . \tag{8}$$

   Furthermore, if $K_{vir} \gg |\frac{1}{G_{se}}|$,

$$\frac{X_m}{F_h} \approx \frac{G_{se}}{s_p s_f} \approx \frac{1}{K_s s_p s_f}. \tag{9}$$

2. If $|m_m s^2 + c_m s| \gg K_{vir} s_p s_f$ (high frequencies),

$$\frac{X_m}{F_h} \approx \frac{1}{m_m s^2+c_m s} \quad . \tag{10}$$

Equation (9) indicates that the teleoperation scheme provides telepresence if

$$K_{vir} \gg \left|\frac{1}{G_{se}}\right|. \tag{11}$$

If the master device is light and frictionless, this first frequency range is quite wide. Telepresence highly depends on G_{se}, as the frequency range of telepresence varies directly with the bandwidth of the force control. However, the teleoperation scheme cannot provide perfect telepresence. Equation (8) shows that

$$\frac{X_m}{F_h} \approx \frac{1}{K_{vir}s_p s_f}, \tag{12}$$

if

$$K_{vir} \ll \left|\frac{1}{G_{se}}\right|, \tag{13}$$

i.e. merely the virtual spring is felt when the environment is much stiffer than K_{vir}. Also, (10) explains that a human operator feels only the master device at high frequencies (e.g. impacts).

Stability. The characteristic equation Δ of X_m/F_h is

$$\begin{aligned} \Delta &= (m_m s^2 + c_m s)(K_{vir} + \tfrac{1}{G_{se}}) \\ &\quad + K_{vir} s_p s_f \tfrac{1}{G_{se}} \\ &= (m_m s^2 + c_m s)\tfrac{1}{G_{se}} \\ &\quad + K_{vir}(m_m s^2 + c_m s + s_p s_f \tfrac{1}{G_{se}}). \end{aligned} \tag{14}$$

K_{vir} and G_{se} determine the stability. Equation (14) indicates that X_m/F_h is stable for any K_{vir} because G_{se} is a stable minimum system with a constant DC value. However, the large value of K_{vir} requires the slave robot to move faster and farther especially in free space. This can cause instability due to the physical limitation of the robot. Thus, the virtual spring was set to

$$K_{vir} = 1000 \text{ [N/m]}, \tag{15}$$

to guarantee stability in free space (obtained experimentally).

The haptics workspace is projected to the PUMA by s_p (Figure 2). s_f scales the reflecting force. In our experiment, these values were chosen as

$$s_p = 2.0 \quad \text{and} \quad s_f = 0.1, \tag{16}$$

considering the range of manipulation, the maximum magnitude of the force sensor, and the maximum forces that the haptics device can produce.

4 Force Controller

This section describes the force control for the PUMA robot. A decoupled force controller is designed for each Cartesian dimension. The AOB provides a straightforward formalism to address state estimation, disturbance compensation and state space control. Stiffness adaptation is necessary to guarantee robustness if the system stiffness changes.

4.1 Manipulator Dynamics

The dynamic equation of a robotic manipulator is described by

$$A\ddot{q} + b(q,\dot{q}) + g(q) + J^T F_c = \Gamma, \tag{17}$$

where the Jacobian, the joint angles, the mass matrix, the Coriolis/centripetal forces and the gravity are respectively given by J, q, A, b and g. F_c denotes the contact force at the end-effector of the manipulator. Using the operational space formulation [6], (17) can be written in Cartesian coordinates as

$$\Lambda\ddot{x} + \mu(q,\dot{q}) + p(q) + F_c = F, \tag{18}$$

$$\Lambda^{-1} = JA^{-1}J^T, \tag{19}$$

$$\mu = J^{-T}b - \Lambda\dot{J}\dot{q} \tag{20}$$

and

$$p = J^{-T}g(q). \tag{21}$$

4.2 Decoupled Force Control

From (18), if[5]

$$F = \hat{F}_c + \hat{\Lambda}F^* + \hat{\mu} + \hat{p}, \tag{22}$$

[5]The symbol $\hat{}$ means estimation.

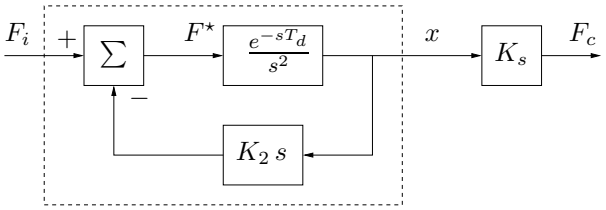

Figure 3: *System Plant (open loop).*

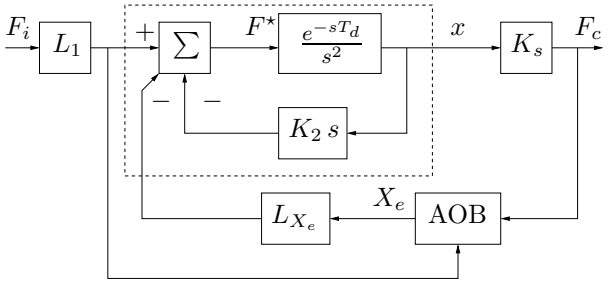

Figure 4: *Closed Loop Force Control with AOB.*

a decoupled system plant appears. The desired plant is then

$$I\ddot{x} = F^*. \tag{23}$$

Figure 3 represents the overall system plant $G(s)$, including a damping factor K_2 and the system stiffness K_s. The dead-time T_d is obtained experimentally. In our setup, it is

$$T_d = 3h, \tag{24}$$

where the sampling time $h = 1.7$ [ms]. Since T_d is small, $G(s)$ can be approximated by

$$G(s) \approx \frac{K_s\, e^{-sT_d}}{s(s + K_2)}. \tag{25}$$

K_2 is computed to achieve an open loop time constant $\tau_o = 0.025$ [s]. Its value is $K_2 = 80$.

4.3 Active Observer Design

Knowing the system plant (25), the theory of active observers introduced in [1] can be applied in a straightforward way to achieve robust adaptive control in the presence of uncertainties. The AOB uses a probabilistic approach to estimate the system state and its disturbances. The method has a systematic formulation, is mathematically elegant and uses the stochastic (Kalman) theory to optimize its performance. Only discrete state space methods are used in the AOB. One of the AOB goals is to provide a stochastic formalism to compensate unmodeled terms using state space techniques. Details of the AOB design can be seen in [3]. Figure 4 illustrates the AOB in the control loop. The state X_e is composed by the force, force derivative, delayed command efforts (due to dead-time), and an active state that compensates disturbances referred to the system input. Stochastic estimation strategies are associated to each state. The model for F_c is poorly known, since K_s may have unpredictable changes. Hence, a sensor based strategy is used to estimate F_c. The estimates are mainly based on measures, giving little importance to the model. The active state, which is a mathematical quantity, also has an uncertain model, coded in the system noise matrix (Kalman filter design). All the other states have accurate models. Hence, their estimates are model based. The state feedback gain L is computed by Ackermann's formula to achieve a critically damped system ($\zeta = 1$) with a closed loop time constant τ_c three times slower than τ_o, i.e. $\tau_c = 3\tau_o$. The extra poles due to dead-time are mapped at $z = 0$. The closed loop settling time is about $5 \times \tau_o$ (0.375 [s]), which is adequate for human-controlled tasks.

This control architecture is kept even for free space conditions (no control switching). In this case, the state estimates are close to zero (except for the active state) and $\dot{x}$ is commanded by F_i.

5 Stiffness Adaptation

Teleoperation tasks involving contact may have abrupt and large changes in K_s. On-line stiffness adaptation must be fast enough to cope with these changes. Hence, the estimation of K_s is crucial in the control design. If K_s is stiffer than the nominal value (i.e. the one used in the force controller), the system response may become unstable. In contrast, if K_s is softer than the nominal value, the system responds slowly. Therefore, adapting the stiffness parameter is necessary to attain high performance.

5.1 Stiffness Adaptation Algorithm

The difference between the measured and estimated force (f_m and f_e respectively) gives useful information about K_s. If the mismatch is large, it indicates that the model is inaccurate[6]. There are two cases:

1. K_s is larger than the nominal stiffness.
2. K_s is smaller than the nominal stiffness.

Figure 5 illustrates the first case: the system may become unstable such that f_m fluctuates around f_e. The difference between the desired force f_d and f_e is relatively small compared to the difference between

[6]The robotic parameters are fairly known. Thus, model errors result from poor K_s estimates.

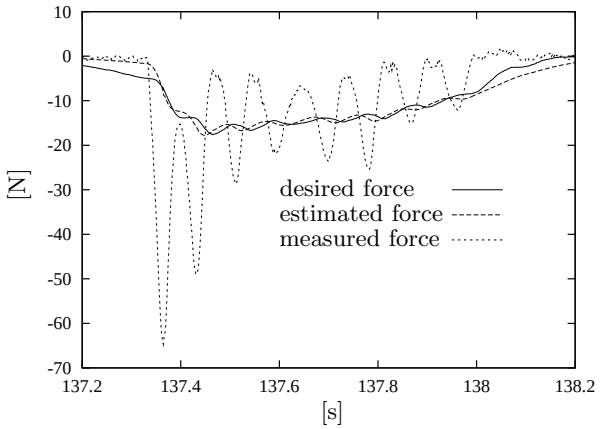

Figure 5: *Force control data without adaptation. Nominal stiffness is* 100 *[N/m] and K_s changes from free space to* 3000 *[N/m].*

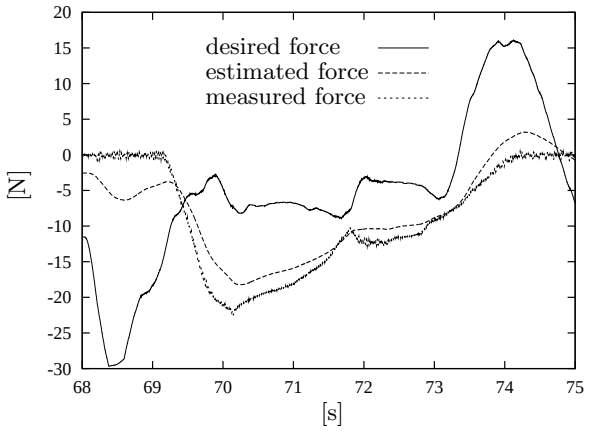

Figure 6: *Force control data without adaptation. Nominal stiffness is* 3000 *[N/m] and K_s changes from free space to* 300 *[N/m].*

f_m and f_e. In the second case, represented in Figure 6, the system response is sluggish. Therefore, the difference between f_d and f_e is bigger than between f_m and f_e.

Based on these results, the following adaptation law is proposed:

$$K_{s,1}^i = K_{s,1}^{i-1} + \Delta\hat{K}_{s,1}^i, \tag{26}$$

where

$$\Delta\hat{K}_{s,1}^i = k_1|f_m - f_e|\,\sigma_d\left(c, \frac{|f_m - f_e|}{|f_e| + a_1} - b_1\right) - k_2|f_d - f_e|\,\sigma_d\left(c, \frac{|f_d - f_e|}{|f_e| + a_2} - b_2\right), \tag{27}$$

$$\sigma_d(c, x) = \frac{1}{1 + e^{-cx}}. \tag{28}$$

$k_1, k_2, a_1, a_2, b_1, b_2$ and c are positive parameters. The upper script i denotes the discrete time step. The first term of the right hand side in (27) corrects errors due to the first case, i.e. it increases $\hat{K}_{s,1}$. The second term, followed by k_2, corrects errors from the second case. The general sigmoid function $\sigma_d(c, x_1 - x_2)$ present in (27) acts as a smooth switch of x_1 centered around x_2. The parameter c defines the smoothing factor. a_1 and a_2 avoid ill-conditioned results when f_e is close to zero. The minimum value of $\hat{K}_{s,1}$ is set to 0 N/m as a saturation function since the stiffness must be non-negative.

Moreover, off-line analysis have shown that the object stiffness increases with the applied force. Equation (29) adjusts the stiffness for this problem,

$$\hat{K}_{s,2} = K_{min} + k_3\,\sigma_d\left(c_0, |f_m - f_0|\right), \tag{29}$$

where f_0, c_0 and k_3 are positive parameters. f_0 indicates the force from which $\hat{K}_{s,2}$ is increased, and K_{min} is the minimum stiffness of $\hat{K}_{s,2}$.

Finally, low-pass filters are used to prevent jerking motions due to quick changes in the stiffness estimation. The filter should not introduce too much time lag; otherwise, the human operator may feel a "sticky" behavior when the contact is released. The filter equations are

$$\hat{K}_{s,1}^{f,i} = \hat{K}_{s,1}^{f,i-1} + l_1(\hat{K}_{s,1}^i - \hat{K}_{s,1}^{f,i-1}) \tag{30}$$

and

$$\hat{K}_{s,2}^{f,i} = \hat{K}_{s,2}^{f,i-1} + l_2(\hat{K}_{s,2}^i - \hat{K}_{s,2}^{f,i-1}). \tag{31}$$

where the upper script i denotes the time step.

The final stiffness adaptation algorithm given by (32) is the sum of (30) and (31)

$$\hat{K}_s^i = \hat{K}_{s,1}^{f,i} + \hat{K}_{s,2}^{f,i}. \tag{32}$$

The minimum value of $\hat{K}_s^i$ is K_{min} from (29). Stiffness values that are too small may lead the system to instability, since the real system stiffness in free motion may be greater. In our experiments, $K_{min} = 100$ [N/m]. All other parameters are shown in Table 1.

a_1	1.0	f_0	20.0	[N]
a_2	0.1	k_1	10.0	[m^{-1}]
b_1	1.5	k_2	10.0	[m^{-1}]
b_2	1.0	k_3	3000.0	[N/m]
c	5.0	l_1	0.05	
c_0	0.2	l_2	0.02	

Table 1: *Numerical values of the design parameters for stiffness adaptation.*

Note that $\hat{K}_{s,1}$ depends on f_e, which is computed from an active observer (AOB) in the force control. Since the f_e value depends on the estimation strategy, Table 1 is correlated with the AOB design.

6 Experimental Results

Force control stability depends on the accuracy of the model[1]. In our setup, it can be shown that stability is assured if the nominal stiffness does not deviate too much from the real one (maximum mismatch is approximately three times softer). Hence, stiffness adaptation is mandatory to guarantee robustness in teleoperation tasks.

Figure 7 shows a teleoperation experiment using a PID force controller on three contact surfaces: a sponge, a book and a table, with free space transitions[7]. The gains for the PID force controller were chosen experimentally such that the bandwidth and the performance of the force controller were maximized ensuring stability at hard contact. However, the bandwidth of the force controller varies for different contacts because the fixed gains are used when the slave system itself is changed. The system responded well in the soft contact (region 1 in Figure 7); however, the contact forces on the hard surfaces were marginally stable (region 2 and 3 in Figure 7). Also, the bandwidth at free space motion was too small; thus, the human operator could significantly feel the position errors and this made it difficult to manipulate the slave robot. This result re-emphasizes the need for stiffness adaptation and robust control scheme for varying stiffness.

Figure 8 shows the same experiment as in Figure 7 using the current force control method. Measured and estimated forces closely match the desired force independent of the contact surface. In free space motion, the slave robot tracks the master position with a designed high bandwidth; thus, the user only feels very small drag. This significantly improved performance of force control in contact and motion tracking in free space achieved much better telepresence.

In Figure 8(b), the stiffness estimation is proportional to the real stiffness, and in free space it reaches the minimum value of 100 [N/m]. Off-line stiffness identification using indirect methods[8] is done to verify the estimation (e.g. some force controllers without integral actions have steady state errors proportional to stiffness mismatches). The identified stiffnesses for the sponge, book and table are represented in Table 2.

[7]The measured force data in free space is not zero due to the gripper inertia.

[8]Direct methods give poor results, particularly for very stiff surfaces, due to sensor noises and encoder resolutions.

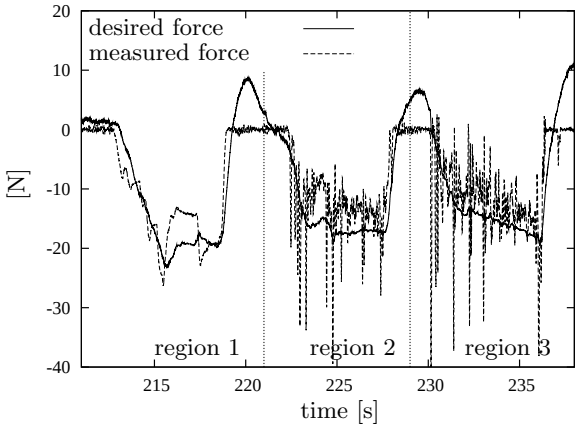

Figure 7: *Teleoperation data with a PID force control in the z direction. Sponge contact (region 1). Book contact (region 2). Desk contact (region 3).*

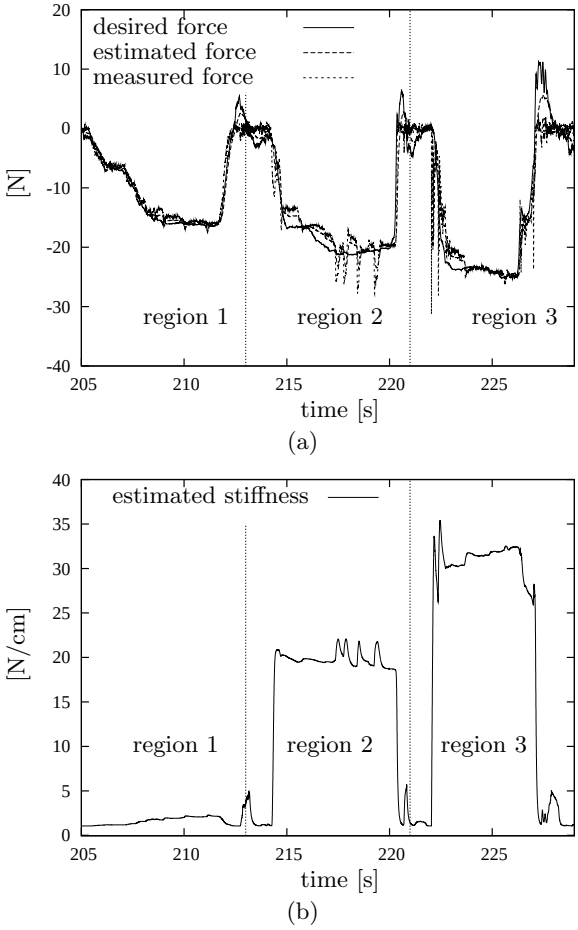

Figure 8: *Teleoperation data with the AOB and adaptation in the z direction. Sponge contact (region 1). Book contact (region 2). Desk contact (region 3). (a) force data. (b) estimated stiffness.*

	sponge	book	desk
K_s [N/m]	300	3000	6000

Table 2: *Off-line stiffness identification (indirect method).*

7 Conclusions

A new teleoperation method for compliant motion tasks is proposed in this paper. A position-position architecture is used, with modifications. Position errors are converted into desired forces through a virtual spring. These forces are sent to the master and slave devices. On the slave side, the force controller applies the AOB theory linked with on-line stiffness estimation without control switching. The control architecture is kept, even for free space conditions. The adaptive force controller achieved good telepresence for various environments.

Only force signals are used to estimate the stiffness (measured, desired and estimated forces). Sigmoid functions, on-line filtering and off-line analysis are important to tune the stiffness estimation parameters.

Experimental results have shown good performance in contact with soft and stiff surfaces. The magnitude of the virtual spring was limited by the free space response of the slave robot. The telepresence can be improved if the larger value of the virtual spring is used for the stiff environment. In the future, the estimated stiffness will be used for designing the virtual spring.

References

[1] R. Cortesão. *Kalman Techniques for Intelligent Control Systems: Theory and Robotic Experiments*. PhD thesis, University of Coimbra, 2002. (submitted).

[2] R. Cortesão, R. Koeppe, U. Nunes, and G. Hirzinger. Explicit force control for manipulators with active observers. In *Proc. of the Int. Conf. on Intelligent Robots and Systems (IROS)*, volume 2, pages 1075–1080, Japan, 2000.

[3] R. Cortesão, R. Koeppe, U. Nunes, and G. Hirzinger. Stochastic active observers: Active state analysis - theory and a robotic force control application. In *Proc. of Int. Conf. on Advanced Robotics (ICAR'01)*, pages 79–84, Hungary, 2001.

[4] R. Daniel and P. McAree. Fundamental limits of performance for force reflecting teleoperation. *International Journal of Robotics Research*, 17(8):811–830, August 1998.

[5] K. Hashtrudi-Zaad and S.E Salcudean. Transparency in time-delayed systems and the effect of local force feedback for transparent teleoperation. *Int. J. on Robotics and Automation*, 18(1):108–114, February 2002.

[6] O. Khatib. A unified approach for motion and force control of robot manipulators: The operational space formulation. *Int. J. on Robotics and Automation*, 3(1):43–53, February 1987.

[7] W.S. Kim, B. Hannaford, and A.K. Bejczy. Force-reflecting and shared compliant control in operating telemanipulators with time delay. *Int. J. on Robotics and Automation*, 8:176–185, April 1992.

[8] D. Lawrence. Stability and transparancy in bilateral teleoperation. *IEEE Trans. on Robotics and Automation*, 9(5):624–637, October 1993.

[9] G. Niemeyer and J. Slotine. Stable adaptive teleoperation. *IEEE Journal of Oceanic Engineering*, 16(1):152–162, January 1991.

[10] M. Zhu and S.E Salcudean. Achieving transparency for teleoperator systems under position and rate control. In *IEEE/RSJ International Conference on Intelligent Robots*, volume 2, pages 7–12, Pittsburgh, PA, 1995.